ELSEVIER

Thin Solid Films 368 (2000) 41–48

thin solid films

www.elsevier.com/locate/tsf

Correlation of the optical gap of $(Ba,Sr)_yTiO_{2+y}$ thin films with film composition

L.D. Rotter[a,*], M.D. Vaudin[a], J.E. Bonevich[a], D.L. Kaiser[a], Soon Oh Park[b]

[a]*Materials Science and Engineering Laboratory, National Institute of Standards and Technology, 100 Bureau Drive, Gaithersburg, MD 20899, USA*
[b]*Semiconductor R&D Center, Samsung Electronics Co. Ltd., Kyungki, South Korea*

Received 4 November 1999; received in revised form 16 January 2000; accepted 16 January 2000

Abstract

A series of 26 $(Ba_{1-x}Sr_x)_yTiO_{2+y}$ thin films with $0.22 \leq y \leq 1.01$ and $x < 0.07$ were grown by metalorganic chemical vapor deposition. Most of the films with $0.22 \leq y \leq 0.37$ were fully amorphous, whereas the films with $0.43 \leq y < 1$ were composed of crystalline (Ba,Sr)-TiO_3 and a Ti-rich amorphous phase. Transmission spectra were measured and analyzed to determine the optical constants of the films, including the optical gap, which was found to decrease as y increased. An effective medium model was used to estimate the volume fraction of amorphous material in the two-phase films from the transmission spectra, by assuming that the two phases each had a fixed optical gap.

Keywords: Amorphous materials; Dielectrics; Optical properties; Optical spectroscopy; Oxides

1. Introduction

There has been a great deal of interest recently in barium strontium titanate $(Ba_{1-x}Sr_x)TiO_3$ (BST) for both electronic and photonic applications. When $x \geq 0.3$, BST is a paraelectric phase at room temperature. The composition $Ba_{0.7}Sr_{0.3}TiO_3$ is being developed for dynamic random access memory (DRAM) devices [1] because of its high dielectric constant. When $x \approx 0$, BST is a ferroelectric phase at room temperature and is of interest for ferroelectric RAM (FeRAM) devices [2] because of its switchable spontaneous polarization, and for photonic applications [3,4] because of its high electro-optic coefficient.

In $(Ba_{1-x}Sr_x)_yTiO_{2+y}$ films with $y < 1$, an amorphous phase either coexists with the crystalline BST phase or comprises the entire film [5,6]. Amorphous phases can form as a result of nonstoichiometry ($y < 1$) in a film, or as a result of low deposition temperatures. Nonstoichiometry in a film may result from the intentional or unintentional variation of process conditions. The presence of an amorphous phase can have a detrimental effect on the dielectric and light scattering properties of the film [7]. It would be advantageous to have a quantitative and nondestructive determination of the amorphous content of such films. Toward that end we have observed that the position of the Urbach edge of $(Ba_{1-x}Sr_x)_yTiO_{2+y}$ films containing a small amount of Sr as an impurity ($0.01 < x < 0.07$) shifts to higher energy as y decreases and may provide an indication of the amorphous content of the films.

2. Experimental

$(Ba_{1-x}Sr_x)_yTiO_{2+y}$ films were grown by metalorganic chemical vapor deposition on 12 mm × 12 mm cleaved (100) single crystal MgO and fused quartz substrates at temperatures of 600 to 800°C [5]. The concentrations of Ba, Sr, and Ti were determined by wavelength dispersive X-ray spectrometry (WDS) in an electron microprobe with polycrystalline $BaTiO_3$ and SrS standards. The spatial resolution of the electron microprobe was insufficient to analyze multiple phases in a film individually, so the measurements gave the average composition. The oxygen concentration was not determined, but because the films were highly transparent in the visible and infrared spectral regions, we assumed the oxygen stoichiometry was near $2 + y$ [8]. Conventional θ–2θ X-ray diffraction (XRD) measurements were made in the range $20° \leq 2\theta \leq 73°$ to identify the crystalline phases present in each film. Three films, one each with $y = 0.55$ (film L), 0.70 (film V), and 1.01 (film Z), were also examined by conventional and high resolution transmission electron microscopy.

Optical transmission spectra were obtained at room

* Corresponding author. Tel.: +1-301-975-6603; fax: +1-304-975-5334.
E-mail address: lrotter@nist.gov (L.D. Rotter).

0040-6090/00/$ - see front matter
PII: S0040-6090(00)00713-6

temperature (21°C) in the energy range 4.13 eV $> E >$ 0.50 eV (wavelength range 0.3 μm $< \lambda <$ 2.5 μm) using a Cary 14 spectrophotometer. In the high energy region the transmittance was often below the noise level of 0.2%. The highest energy E_{max} for which reliable transmittance data was obtained varied from film to film. Variations in the film thickness produced fringes of equal chromatic order near the edges of the films. A 4.0-mm diameter aperture was placed over the center of the central fringe to minimize the effect of film thickness variation on the spectra.

3. Results

The y (molar ratio (Ba + Sr)/Ti) values of the films calculated from the WDS results ranged from 0.22 to 1.01; the x (molar ratio Sr/(Ba + Sr)) values ranged from 0.01 to 0.07. Uncertainties (1σ) of ±0.05 in y and ±0.01 in x were estimated taking into account uncertainties in the measurement conditions, data reduction algorithms and film thicknesses.

Conventional θ–2θ XRD patterns showed only peaks indexed to crystalline BST for films with $y \geq 0.43$; film D with $y = 0.34$ displayed only one weak peak which corresponded to the 200 peak of BST. Most of the films had $y < 1$ ($y = 1$ being stoichiometric BST), so the films contained a Ti-rich non-diffracting phase in addition to crystalline BST. Transmission electron microscopy studies revealed that this non-diffracting phase was amorphous [5]. For the three films studied, the amorphous fraction was found to decrease as y increased; only a small amount of amorphous phase in isolated ~1 nm size regions was observed in the film with $y = 1.01$ (film Z). For all but one of the films with $y < 0.37$, no peaks were observed in the XRD patterns, indicating that those films were fully amorphous.

A typical optical transmission spectrum is shown in Fig. 1a. Each spectrum was fit with a model [9], referred to here as the single phase model (SPM), which assumed that the film was a single homogeneous slab on a thick substrate of known refractive index (for MgO: Ref. [10]; for fused quartz: Ref. [11]). The parameters of the SPM included the complex refractive index $\tilde{n} = n + ik$ of the film with four parameters, E_d, E_0, E_U, and E_G, described below, as well as film thickness, surface roughness, and thickness inhomogeneity. n was modeled with a two parameter Sellmeier equation [12]

$$n^2 = 1 + E_d E_0/(E_0^2 - E^2) \tag{1}$$

where E is the photon energy, E_d is the dispersion energy, E_0 is an average oscillator energy, and the oscillators are approximations to the important interband transitions in the Brillouin zone [12].

In order to determine the functional form of k we approximated the absorption coefficient $\alpha = 4\pi k/\lambda$ by

$$\alpha \approx (1/t)\ln\left[1 + \frac{1/T(\alpha) - 1/T(0)}{\langle 1/T(0)\rangle}\right] \tag{2}$$

where t is the film thickness, $T(\alpha)$ is the transmittance of the substrate coated with a film, $T(0)$ is the SPM fit to $T(\alpha)$ with α set equal to zero, and $\langle\rangle$ indicates an average over energy. $T(0)$ is determined by an SPM fit to the data in the transparent region of the spectrum and is extrapolated into the absorbing region of the spectrum. Eq. (2) gives an approximate correction for the effect of reflections at the interfaces (L.H. Robins, unpublished; an alternate method can be found in Ref. [9]).

A typical absorption coefficient spectrum $\alpha(E)$ calculated by applying Eq. (2) to the data in Fig. 1a is shown in Fig. 2a. The exponential dependence of α on E is clear, indicating that k should be modeled with an Urbach edge (see e.g. Ref. [13] and references therein)

$$k = (hc/4\pi E)(10^4\ \mathrm{cm}^{-1})\exp[(E - E_G)/E_U] \tag{3}$$

where E_G is the optical gap which we arbitrarily defined as the energy where the absorption coefficient $\alpha = 4\pi k/\lambda$ reaches a conveniently measured value of $10^4\ \mathrm{cm}^{-1} = 1\ \mu\mathrm{m}^{-1}$, and E_U is the Urbach energy, which is given by the slope of the absorption edge.

As further verification that the data in Fig. 2a should be modeled with an Urbach edge (Eq. (3)) and not a Tauc bandgap function (see e.g. Ref. [13], Section 3-A-1,2)

$$E\alpha(E) = \begin{cases} A(E - E_g)^p & \text{if } E \geq E_g \\ 0 & \text{if } E < E_g \end{cases} \tag{4}$$

where E_g is the bandgap, A is a scale factor, and p is an exponent usually between 0.5 and 2, we plotted $[E\alpha(E)]^2$ and $[E\alpha(E)]^{1/2}$ versus E. Fig. 2b shows those plots are clearly nonlinear, indicating that Eq. (4) does not accurately describe the data.

In addition to the Urbach edge absorption, six of the

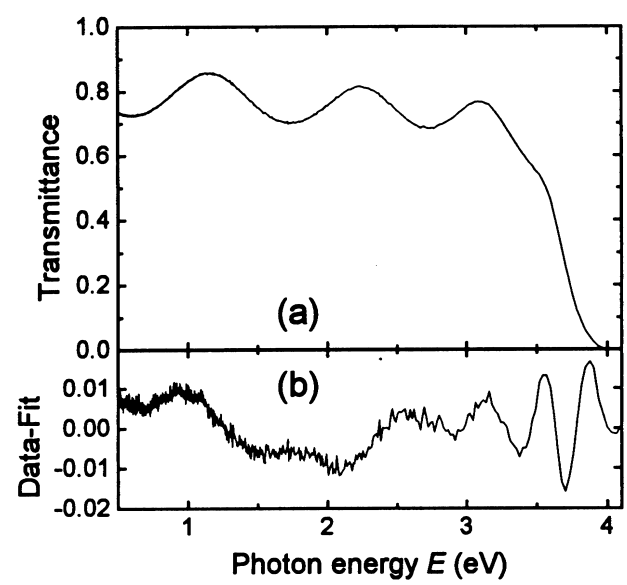

Fig. 1. (a) Transmittance spectra of film S on MgO ($y = 0.72$, $x = 0.02$, thickness = 550 nm). (b) Difference between the data of (a) and the single phase model fit.

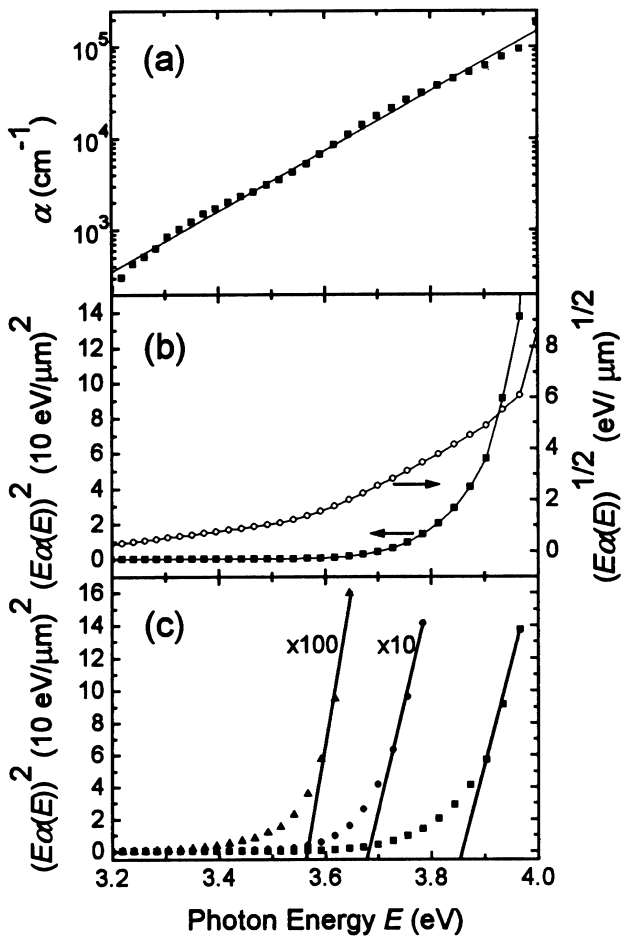

Fig. 2. Various methods of plotting absorption coefficient $\alpha(E)$ versus photon energy E calculated from the transmittance spectra of Fig. 1 using Eq. (2): (a) $\alpha(E)$ versus E, (b) $[E\alpha(E)]^2$ and $[E\alpha(E)]^{1/2}$ versus E, (c) $[E\alpha(E)]^{1/2}$ versus E plotted on three different vertical scales. A common method to determine the bandgap E_g is to linearly extrapolate the high energy portion of such curves as those shown in (b) to $\alpha = 0$ [35]. This method is deceptive in this case. The bandgap determined by this method is dependent on the scale and energy range on which the data are plotted, as shown in c, because the linear portion of the curves covers only a small energy range [36].

seven films with $x \leq 0.37$ (films A, C–G) had a weak absorption throughout the visible and infrared spectral regions. This absorption may be due to carbon impurities in these amorphous films, and was modeled with an absorbance term increasing linearly with energy.

For all the films the data were collected at equal wavelength intervals, but the data were weighted by $1/\lambda$ so that the fitting procedure gave equal weight to equal energy intervals. The fits using Eqs. (1) and (3) yielded E_G, E_U, E_d, and E_0 shown in Figs. 3 and 4, as well as film thicknesses in the range 100–1000 nm, rms surface roughnesses in the range 0–18 nm that were weakly correlated with film thickness [7], and thickness inhomogeneities of < 20 nm over the 4.0 mm diameter illuminated area of the film.

As shown in Fig. 3, there is a trend of decreasing E_G with increasing y. Fig. 4a shows that E_U is not linearly correlated with y but might have a broad maximum about $y = 0.6$. None of the parameters E_d, E_0, or $n_0 = \sqrt{1 + E_d/E_0}$ (the low energy limit of the refractive index) was correlated with y (see Figs. 4b–d), nor were any of the four parameters of $\tilde{n}$ (E_d, E_0, E_G, and E_U) correlated with each other except for a positive correlation of E_d with E_0 as shown in Fig. 5.

None of the parameters of $\tilde{n}$ was correlated with the Sr concentration x. This is not surprising given the similarity between the optical properties of $BaTiO_3$ and $SrTiO_3$ [14] and the small values of x. Measurements of the optical bandgap of $Ba_xSr_{1-x}TiO_3$ films with a $0 < x < 1$ indicate that the difference in bandgap between a $Ba_xSr_{1-x}TiO_3$ film with $x = 0$ and one with $x = 0.07$ (the maximum value for the films studied here) is ~0.05 eV [15], which is small compared to the 0.5 eV range of values shown in Fig. 3. We will therefore not discuss the Sr content further.

The increase in bandgap with decreasing film thickness and decreasing grain size observed in Ref. [16] was not observed in our films (see Table 1). We note that our films are thinner than those in Ref. [16] and that E_G of our films is larger than E_G of bulk $BaTiO_3$ [17]. It may be that the effect is weak or has saturated in films thinner than 1 μm.

4. Discussion

The absorption coefficient spectrum in the Urbach regime (Fig. 2a) is comparable to that found by Onton and Marrello [18] but extends to higher values of α. For crystalline, microcrystalline, and amorphous stoichiometric $BaTiO_3$ their absorbance data show a transition to the Tauc regime,

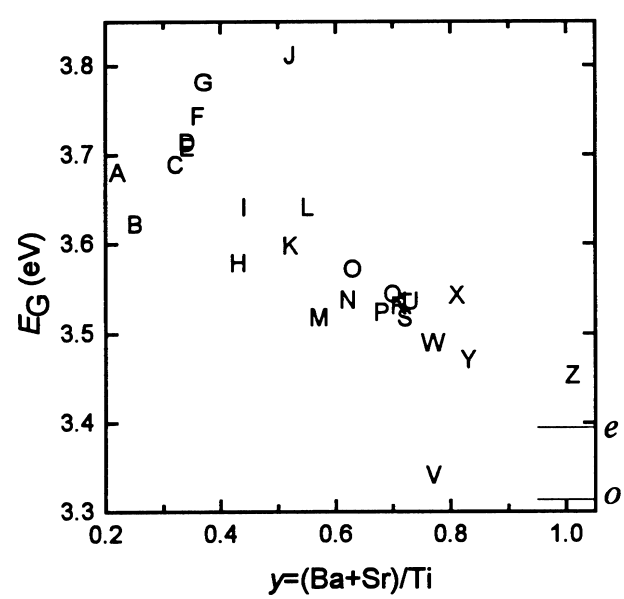

Fig. 3. Optical gap E_G (from Eq. (3)) versus film composition $y = (Ba + Sr)/Ti$. The data points are identified by the corresponding film name (letters A through Z). The long tick marks on the right hand axes indicate the values for ordinary (o) and extraordinary (e) waves in single crystal $BaTiO_3$ according to Ref. [17].

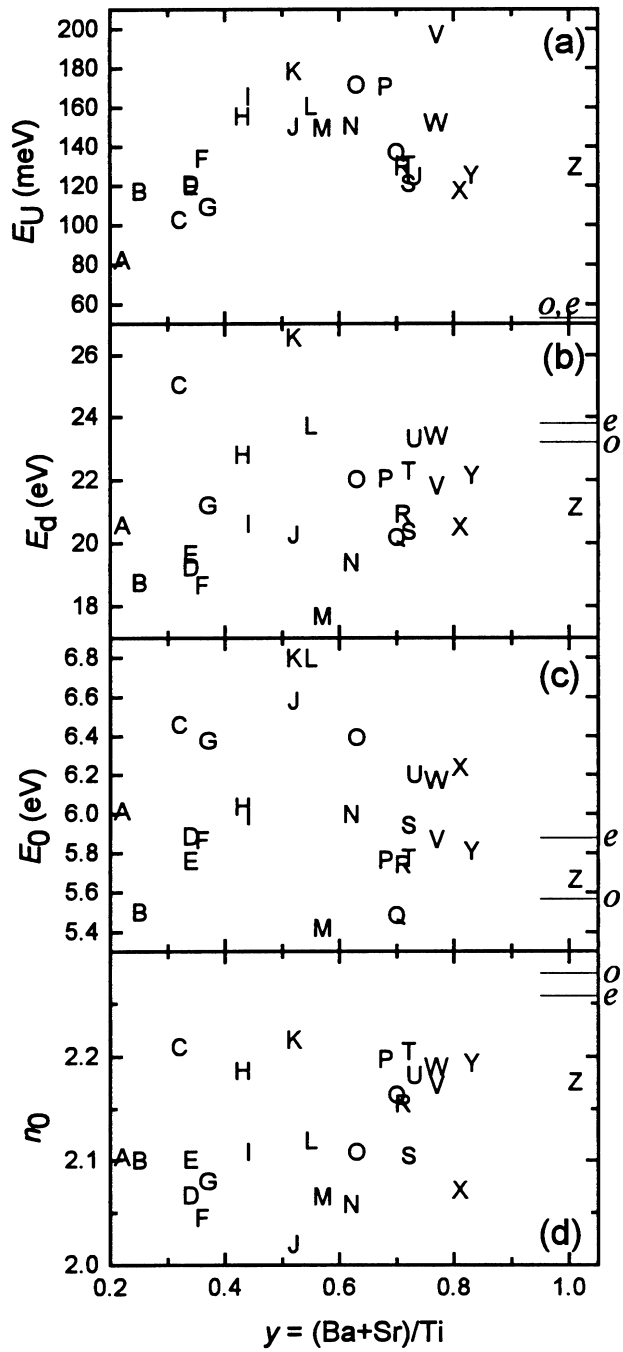

Fig. 4. (a) Urbach energy E_U (from Eq. (3)), (b) dispersion energy E_d (from Eq. (1)), (c) oscillator energy E_0 (from Eq. (1)), and (d) low-energy limit of the refractive index n_0 versus film composition y = (Ba + Sr)/Ti. The data points and the long tick marks on the right-hand axes are identified as in Fig. 3.

i.e. a power law dependence of the absorption coefficient on energy, for $\alpha > 2 \times 10^4$ cm^{-1}, whereas the Urbach edge shown in Fig. 2a extends up to α~10^5 cm^{-1}.

The correlation of E_G with y shown in Fig. 3 is the main result of this work. Fig. 3 allows a rough determination of y from a measurement of E_G (an F-test gave a probability of 6×10^{-6} that the correlation was by chance). We wish to

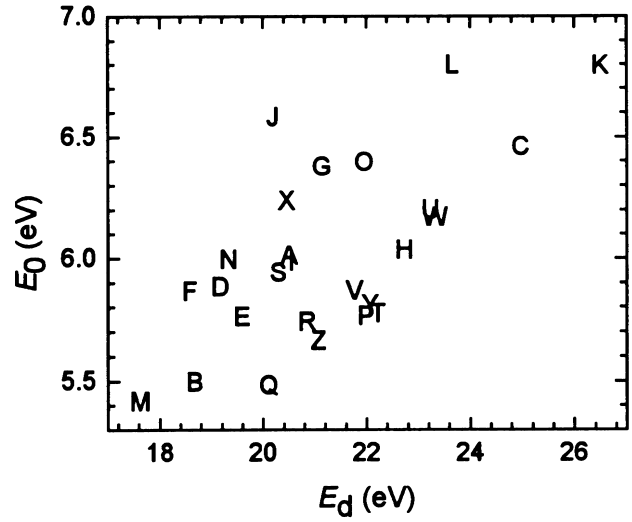

Fig. 5. Oscillator energy E_0 versus dispersion energy E_d (from Eq. (1)) for the complete set of films. An effective medium combination of voids and fully dense material is inconsistent with the positive correlation of E_0 with E_d (see Section 4).

explore now to what extent the phase content of the films can also be determined from E_G.

The microstructure of the films depends upon the composition: most of the films with $y \leq 0.37$ are fully amorphous, whereas the films with $0.43 \leq y < 1$ are a mixture of crystalline BST and an amorphous phase. XRD measurements have shown that the a and c lattice parameters of the crystalline BST phase in the two-phase films are independent of y [5], so it is reasonable to assume that the BST phase has a fixed composition of $y = 1$. In contrast, the composition of the amorphous phase may not be fixed, since Ba_yTiO_{2+y} can be amorphous over the entire composition range $0 \leq y \leq 1$ [19–23]. Thus, as y varies from film to film, either or both of the composition of the amorphous phase and the relative amounts of BST and the amorphous phase are expected to vary.

Before concentrating on the optical gap E_G we will discuss the other parameters of $\tilde{n}$. We would like to suggest mechanisms which would remove the correlation of E_U, E_d, and E_0 with y while leaving the correlation of E_G with y intact. Our point is to demonstrate that this is not an inherently self-contradictory set of data. We are not attempting to use our data to prove that these suggested mechanisms for removing the correlation of E_U, E_d, and E_0 with y are present.

From Fig. 4d we note that for all the films n_0 is lower than for bulk $BaTiO_3$ where $n_0 = 2.29$ [12]. This has been observed previously in amorphous $BaTiO_3$ films [19–21] where it was attributed to the amorphous films being less dense that their crystalline counterparts [19–21], and to the electronic structure changing with the average interatomic spacing [19,21] and atomic coordination [19]. Wöhlecke et al. [19] attribute ~70% of the difference in refractive index between the amorphous and crystalline phases of $BaTiO_3$ to changes in electronic structure. Dispersion in $BaTiO_3$ and

TiO_2 is due to electronic transitions at the Brillouin zone edge, whereas the fundamental bandgap is a zone center transition [14,24]. Thus, changes in electronic structure that change E_d and E_0 with y are not expected to change E_G.

A standard approach to determine the density of a specimen suspected of having voids is to fit the optical constants of the specimen with an effective medium model combining fully dense material and voids. While this approach might work for the stoichiometric film Z under the assumption that the non-void fraction has the same optical constants as bulk crystalline BST, it will not work for the films which have an amorphous component, because we do not have optical constants for the fully dense amorphous phase independent of those measured here. While voids in the films would also reduce n_0, the correlation of E_d with E_0 shown in Fig. 5 is positive, which is inconsistent with the presence of voids. We demonstrate this as follows. If two media with refractive indices of the form of Eq. (1) are combined in an effective medium (EM) which is then fit with a refractive index of the form of Eq. (1), the resulting E_d and E_0 of the EM will interpolate between the respective values for the two media. A clear choice for E_d of void would be zero, so that E_d of the EM would decrease as the volume fraction of void f_v increased. To determine what happens to E_0 of the EM as a function of f_v we solved the problem numerically for several different EM models (for a short review of EM models see Ref. [25]). We found that E_0 of the EM remained constant or increased as f_v increased. For $0 \leq f_v \leq 0.2$ we found E_0 versus E_d was nearly linear with slope -0.005 for Maxwell–Garnett, -0.009 for Bruggeman, 0 for Bragg–Pippard with $L = 0$ (no screening), -0.010 for Bragg–Pippard with $L = 0.5$, and -0.218 for Bragg–Pippard with $L = 1$ (maximum screening). In Fig. 4 the slope of a linear least squares fit to the data is 0.13. For comparison, see Fig. 8 of Ref. [15]. Furthermore, TEM studies showed no evidence of voids.

In pure bulk $BaTiO_3$ $E_U = 53$ meV and is an intrinsic property of the lattice, being due to indirect transitions [26]. In our films E_U is two to four times larger than this value. The increased band tailing leading to the large E_U values is most likely due to structural disorder such as defects and spatially varying composition [27,28]. Film to film variation in defect structures and compositional homogeneity could give the variation of E_U with y observed in Fig. 4a. One defect that would contribute to the high E_U values in the films is oxygen vacancies, which lead to shallow levels in the bandgap [29]. Studies on bulk nonstoichiometric $BaTiO_3$ have shown that the oxygen vacancy

Table 1
Parameter values for the 26 $(Ba_{1-x}Sr_x)_yTiO_{2+y}$ films in this study as well as literature values for single crystal $BaTiO_3$[a]

Film ID	y	x	t (μm)	E_G (eV)	E_U (eV)	E_d (eV)	E_0 (eV)	n_0	f_a
A	0.22	0.067	1.08	3.678	0.081	20.5	6.00	2.101	–
B	0.25	0.059	0.32	3.621	0.116	18.7	5.49	2.098	–
C	0.32	0.065	0.78	3.687	0.101	25.0	6.45	2.207	–
D	0.34	0.052	0.34	3.712	0.120	19.2	5.88	2.064	1.01
E	0.34	0.051	0.33	3.707	0.118	19.6	5.75	2.099	–
F	0.36	0.053	0.34	3.741	0.133	18.6	5.86	2.043	–
G	0.37	0.069	0.60	3.780	0.108	21.1	6.37	2.078	–
H	0.43	0.060	0.16	3.576	0.154	22.7	6.03	2.184	0.60
I	0.44	0.065	0.22	3.639	0.164	20.6	5.98	2.106	0.87
J	0.52	0.058	0.44	3.810	0.149	20.2	6.57	2.018	1.12
K	0.52	0.046	0.58	3.596	0.177	26.5	6.79	2.214	0.74
L	0.55	0.062	0.33	3.639	0.160	23.7	6.79	2.118	0.87
M	0.57	0.048	0.47	3.516	0.148	17.6	5.41	2.063	0.43
N	0.62	0.008	0.49	3.535	0.149	19.3	5.99	2.056	0.53
O	0.63	0.057	0.36	3.570	0.170	22.0	6.39	2.107	0.65
P	0.68	0.052	0.14	3.521	0.170	22.0	5.76	2.195	0.44
Q	0.70	0.051	0.21	3.542	0.136	20.1	5.47	2.162	0.58
R	0.71	0.056	0.28	3.529	0.128	20.8	5.73	2.153	0.53
S	0.72	0.024	0.55	3.515	0.120	20.3	5.93	2.102	0.47
T	0.72	0.065	0.23	3.533	0.130	22.2	5.77	2.203	0.54
U	0.73	0.050	0.39	3.534	0.123	23.2	6.19	2.180	0.56
V	0.77	0.064	0.10	3.339	0.196	21.8	5.86	2.171	−1.08
W	0.77	0.065	0.16	3.487	0.151	23.3	6.16	2.188	0.26
X	0.81	0.042	1.15	3.540	0.116	20.5	6.23	2.070	0.60
Y	0.83	0.066	0.44	3.469	0.124	22.1	5.80	2.192	0.15
Z	1.01	0.062	0.18	3.452	0.128	21.1	5.66	2.174	–
o[b]	1	0		3.314	0.053	23.2	5.57	2.279	0
e[b]	1	0		3.395	0.053	23.8	5.88	2.258	0

[a] t is the film thickness, E_G is the optical gap and E_U is the Urbach energy as given in Eq. (3), E_d is the dispersion energy and E_0 is the oscillator energy as given in Eq. (1), n_0 is the low energy limit of the refractive index, and f_a is the volume fraction of the amorphous phase.
[b] Values for ordinary (o) and extraordinary (e) rays in single crystal $BaTiO_3$ taken from Ref. [17].

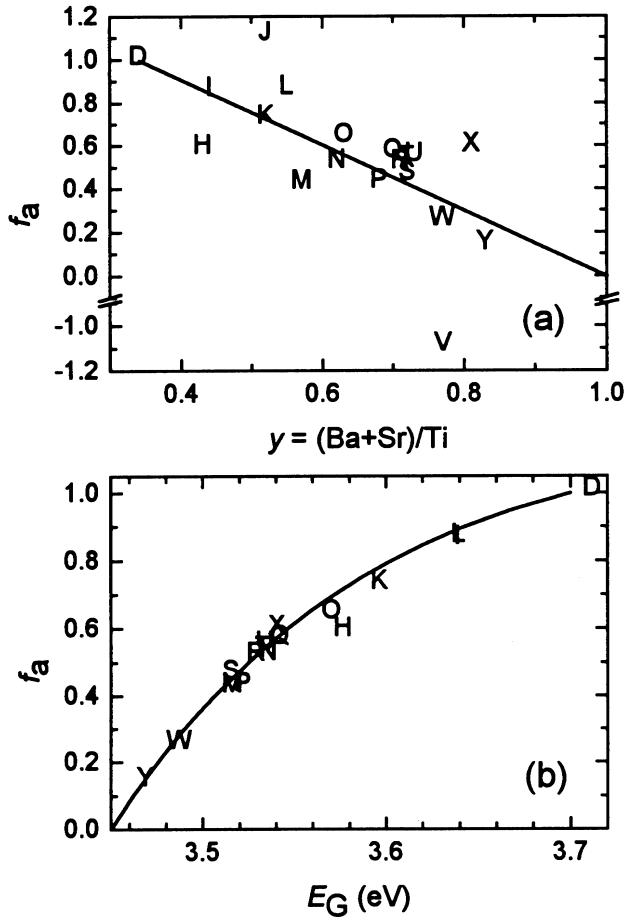

Fig. 6. Volume fraction f_a of amorphous phase material versus (a) composition $y = (Ba + Sr)/Ti$ and (b) optical gap E_G. In a, the dotted lines delineate the physically realistic range $0 \leq f_a \leq 1$. The solid line is a linear interpolation between the points $f_a = 1$ at $y = 0.34$ (i.e. highly Ti enriched, fully amorphous phase) and $f_a = 0$ at $y = 1$ (i.e. stoichiometric fully crystalline BST) and serves as a guide to the eye. The smooth curve in (b) was calculated by numerically solving Eqs. (5) and (6) for f_a at $\alpha(E = E_G) = 10^4$ cm^{-1} using $E_U = 138$ meV, $E_d = 21.3$ eV, and $E_0 = 6.00$ eV, which are the average values of the parameters plotted in Fig. 4a–d.

concentration increases with increasing Ti concentration [30]. A similar effect in our films would result in a decrease in the optical gap E_G with decreasing y, which is the opposite of what we observe in Fig. 3. Therefore oxygen nonstoichiometry is not a likely cause of the observed increase in optical gap with decreasing y.

In general, a shift in E_G indicates either a change in E_U or a change in the oscillator strength (proportional to the scale factor A in Eq. (4)) or bandgap E_g of the fundamental absorption to which the Urbach tail is attached [18], i.e. a change in the Tauc regime (see e.g. Ref. [13], Secs. 3-A-1 and 3-A-2) [31,32] which lies at energies above our experimental range. Since E_U is not correlated with y, the observed decrease in E_G with increasing y (Fig. 3) must be due to an increase in A and/or a decrease in E_g with increasing y. One study on stoichiometric $BaTiO_3$ films has shown that A increases and E_g decreases as the crystallinity increases [18]. Likewise, E_g values for amorphous [22,23] TiO_2 are higher than those for crystalline [24] TiO_2, which has a fundamental band edge structure similar to that of $BaTiO_3$ [14,24]. For our films, TEM results have shown that the amorphous fraction decreases with increasing y [5]. Therefore we will assume that the observed decrease in E_G with increasing y results from a decrease in the fraction of amorphous material in the films with increasing y, and that the crystalline BST and the amorphous phase each have a fixed value of E_G even if the stoichiometry of the amorphous phase changes with y.

These assumptions allowed us to refit the transmission spectra using a two phase effective medium model, referred to here as the EMM fit. Our approach was to select an optical gap value for the crystalline BST and another for the amorphous phase, and then to interpolate between those two optical gaps to get the optical gap of each two-phase film using the volume fraction of the amorphous phase f_a as the interpolation parameter. The average value of the optical gap of the six fully amorphous films (A–C and E–G) with $y \leq 0.37$ was used as the optical gap of the amorphous phase, $E_G^{(a)} = 3.70 \pm 0.05$ eV (the error bar is the standard deviation of the E_G values for the amorphous films A–C and E–G). The optical gap of film Z with $y = 1.01$ was used as the optical gap of the crystalline BST phase, $E_G^{(c)} = 3.45 \pm 0.01$ eV (the error bar represents the difference in E_G values determined by the SPM fit with and without surface roughness).

Numerous effective medium models for the complex refractive index are available. For a brief review see Ref. [25]. We chose to use the Bragg–Pippard effective medium model [33] for the complex refractive index

$$\tilde{n}^2 = \tilde{n}_a^2 + \frac{(1 - f_a)(\tilde{n}_c^2 - \tilde{n}_a^2)}{1 + f_a L(\tilde{n}_c^2 - \tilde{n}_a^2)/\tilde{n}_a^2} \tag{5}$$

with a depolarizing coefficient $L = 0.5$, where $\tilde{n}_c(\tilde{n}_a)$ is the complex refractive index of the crystalline BST (amorphous) phase. Eq. (5) is a good approximation for all values of f_a between 0 and 1 [33]. The choice of $L = 0.5$ is appropriate for a columnar microstructure which has been observed by transmission electron microscopy in other $(Ba_{1-x}Sr_x)_yTiO_{2+y}$ films deposited in our MOCVD system [34]. We tried three alternate effective medium models, including Bragg–Pippard with $L = 1$, Bragg–Pippard with $L = 1/3$ (equivalent to Maxwell–Garnet), and Bruggeman (see Ref. [25]). None qualitatively changed the results.

In order to accommodate the observation that E_G was the only parameter of $\tilde{n}$ correlated with y we made the following unusual assignments for $\tilde{n}_c$ and $\tilde{n}_a$

$$\tilde{n}_j = n + i(hc/4\pi E)(10^4 \text{ cm}^{-1})\exp[(E - E_G^{(j)})/E_U] \qquad j = a, c \tag{6}$$

where $E_G^{(c)}(E_G^{(a)})$ is the optical gap of the crystalline BST (amorphous) phase. That is, for each film to which the EMM was applied, we allowed the parameters of $\tilde{n}$ other

than E_G to remain at the values determined by the SPM fit for that film. The surface roughness, film thickness and thickness inhomogeneity were also fixed at the values determined by the SPM fit. The only variable parameter of the EMM fit was f_a.

As seen in Fig. 6a, there is a trend of decreasing amorphous fraction with increasing y. The two values of f_a outside the range 0 to 1 (for film U $f_a = -1.1$ and for film J $f_a = 1.1$) clearly indicate that our implementation of the effective medium model is not completely successful in describing the data. Either the model is correct, but we have chosen too low a value of $E_G^{(a)}$ and too high a value of $E_G^{(c)}$, or factors other than the amorphous fraction are significantly affecting the value of the optical gap in those films. To the extent that the data in Fig. 6a is linear, the data indicate the composition of the amorphous phase is fixed across the entire composition range of the two-phase films. This further justifies the assumption that the optical gap of the amorphous phase is fixed.

Combining Fig. 6a with the E_G versus y data of Fig. 3 we find the desired relationship between E_G and f_a (see Fig. 6b). Combining Fig. 6a and Fig. 3 in this way is equivalent to solving Eqs. (1), (5) and (6) for $f_a = f_a(E,E_U,E_d,E_0)$ at $E = E_G$ defined by the condition that in Eq. (5) $\mathrm{Im}(\tilde{n}(E = E_G, E_U, E_d, E_0)) = (hc/4\pi E_G)(10^{-4}\ \mathrm{cm}^{-1})$ (cf. Eq. (3)), where Im indicates the imaginary part. The smooth curve in Fig. 6b is the numerical solution $f_a = f_a(E = E_G, E_U, E_d, E_0)$ of Eqs. (1), (5) and (6) with fixed values of E_U, E_d, and E_0. The proximity of the data in Fig. 6b to the smooth curve indicates nothing about the appropriateness of Eqs. (1), (5) and (6), because the data as presented are merely numerical solutions of those equations. The smoothness of the data in Fig. 6b does show that f_a depends only weakly on E_U, E_d, and E_0. Thus, an estimate of f_a could be obtained from a determination of E_G alone combined with estimates of E_U, E_d, and E_0. In practice then, E_G could be determined from transmittance measurements at only two energies in the Urbach regime combined with a thickness measurement from, e.g. a crystal thickness monitor. This value of E_G together with estimates of E_U, E_d, and E_0 could be used in Eqs. (1), (5) and (6) to estimate f_a.

5. Conclusions

In conclusion, we have determined that the optical gap of $(Ba_{1-x}Sr_x)_yTiO_{2+y}$ films composed of Ti-rich amorphous material and/or crystalline BST tends to decrease with increasing y. By using effective medium modeling we have shown that determination of the optical gap can provide quantitative and nondestructive analysis of the amorphous fraction of $(Ba_{1-x}Sr_x)_yTiO_{2+y}$ films if we assume that the crystalline BST and the amorphous phase each have a fixed optical gap. The amorphous fraction so determined was in general accord with TEM results, but in isolated cases nonphysical results were obtained.

In this work data were collected using transmission spectrophotometry, but use of the effective medium model to determine the amorphous content is independent of the means by which the data are collected. Spectroscopic ellipsometry should work as well. Both techniques are available for in-situ monitoring of film growth, allowing the determination of the amorphous content of the films to be done in-situ.

Acknowledgements

The authors thank Dr. L H. Robins of NIST for providing the fitting program used to analyze the data. The use of trade names or brand names does not imply endorsement of the product by the National Institute of Standards and Technology.

References

[1] J.F. Scott, Ferroelectrics 183 (1996) 51.
[2] J.F. Scott, Ferroelectrics Rev. 1 (1998) 1.
[3] A.M. Glass, Science 235 (1987) 1003.
[4] R.L. Holman, L.M. Althouse Johnson, D.P. Skinner, Opt. Eng. 26 (1987) 134.
[5] D.L. Kaiser, M.D. Vaudin, L.D. Rotter, J.E. Bonevich, I. Levin, J.T. Armstrong, A.L. Roytburd, D.G. Schlom, J. Mater. Res. 14 (1999) 4657.
[6] I. Levin, R.D. Leapman, D.L. Kaiser, P.C. van Buskirk, S. Bilodeau, R. Carl, Appl. Phys. Lett. 75 (1999) 1299.
[7] D.K. Fork, F. Armani-Leplingard, J.J. Kingston, MRS Bull. 21 (1996) 53.
[8] J.Y. Chang, M.H. Garrett, H.P. Henssen, C. Warde, Appl. Phys. Lett. 63 (1993) 3598.
[9] L.H. Robins, E.N. Farabaugh, A. Feldman, Diam. Films Technol. 5 (1995) 199.
[10] D.M. Roessler, in: E.D. Palik (Ed.), Handbook of Optical Constants of Solids II, Academic Press, San Diego, CA, 1991, p. 919.
[11] H.R. Phillip, in: E.D. Palik (Ed.), Handbook of Optical Constants of Solids, Academic Press, San Diego, CA, 1985, p. 749.
[12] S.H. Wemple, M. DiDomenico Jr., Phys. Rev. B 3 (1971) 1338.
[13] J.I. Pankove, Sec. 3-A-5, Optical Processes in Semiconductors, Dover, New York, 1971.
[14] M. Cardona, Phys. Rev. 140 (1965) A651.
[15] R. Thielsch, K. Kaemmer, B. Holzapfel, L. Schultz, Thin Solid Films 301 (1997) 203.
[16] J.S. Zhu, X.M. Lu, W. Jiang, et al., J. Appl. Phys. 81 (1997) 1392.
[17] S.H. Wemple, M. DiDomenico Jr., I. Camlibel, J. Phys. Chem. Solids 29 (1968) 1797.
[18] A. Onton, V. Marrello, in: G. Lucovsky, F.L. Galeener (Eds.), Structure and Excitations of Amorphous Solids, American Institute of Physics Conference Proceedings, 31, 1976, p. 320.
[19] M. Wöhlecke, V. Marrello, A. Onton, J. Appl. Phys. 48 (1977) 1748.
[20] P. Li, J.F. McDonald, T.-M. Lu, J. Appl. Phys. 71 (1992) 5596.
[21] W.-T. Liu, S.T. Lakshmikumar, D.B. Knorr, E.J. Rymaszewski, T.-M. Lu, Appl. Phys. Lett. 66 (1995) 809.
[22] K. Fukushima, I. Yamada, T. Takagi, J. Appl. Phys. 58 (1985) 4146.
[23] M. Takeuchi, Phys. Status Solidi. A 55 (1979) 653.
[24] M. Cardona, G. Harbeke, Phys. Rev. A 137 (1965) 1467.
[25] A. Feldman, E.N. Farabaugh, W.K. Haller, D.M. Sanders, R.A. Stempniak, J. Vac. Sci. Technol. A 4 (1986) 2969.
[26] S.H. Wemple, Phys. Rev. B 2 (1970) 2679.

[27] G.D. Cody, T. Tiedje, B. Abeles, B. Brooks, Y. Goldstein, Phys. Rev. Lett. 47 (1981) 1480.
[28] S.M. Wasim, G. Marín, C. Rincón, G. Sánchez Perez, A.E. Mora, A. E. Mora, J. Appl. Phys. 83 (1998) 3318.
[29] C.N. Berglund, H.J. Braun, Phys. Rev. 164 (1967) 790.
[30] N.-H. Chan, R.K. Sharma, D.M. Smyth, J. Am. Ceram. Soc. 64 (1981) 556.
[31] L.H. Robins, J.R. Lowney, D.K. Wickenden, J. Mater. Res. 13 (1998) 2480.
[32] H. Okamoto, K. Hattori, Y. Hamkawa, J. Non-Cryst. Solids 198–200 (1996) 124.
[33] W.L. Bragg, A.B. Pippard, Acta Cryst. 6 (1953) 865.
[34] D.L. Kaiser, M.D. Vaudin, G. Gillen, C.-S. Hwang, L.H. Robins, L.D. Rotter, in: S.V. Desu, D.B. Beach, B.W. Wessels, S. Gokoglu (Eds.), Metalorganic Chemical Vapor Deposition of Electronic Ceramics, Fall 1993, MRS Symp. Proc., 335, 1994, p. 47.
[35] D.E. Sweenor, S.K. O'Leary, B.E. Foutz, Solid State Commun. 110 (1999) 281.
[36] R.M. Dawson, Y.M. Li, M. Gunes, et al., in: M.J. Thompson, Y. Hamakawa, P.G. LeComber, A. Madan, E.A. Schiff, et al. (Eds.), Amorphous Silicon Technology, Spring 1992, MRS Symp. Proc., 258, 1992, p. 595.